# The molecular beam electric resonance spectrum of $OPF_3$

W. Leo Meerts, Irving Ozier,[1] and Antoni Dymanus

*Fysisch Laboratorium, Katholieke Universiteit, Toernooiveld, Nijmegen, The Netherlands*

Received February 23, 1979

The molecular-beam electric resonance spectrum of phosphoryl fluoride ($^{16}OPF_3$) has been investigated. A hyperfine study of ($K = 0$) multiplets has been combined with earlier magnetic resonance data and chemical shift arguments to obtain four spin–rotation constants and two tensor spin–spin constants. The results (in kHz) are: $c_\perp^P = +7.7(8)$, $c_\parallel^P = +21(6)$, $c_\perp^F = +4.6(4)$, $c_\parallel^F = +4.0(2.5)$, $d^{PF} = -2.3(9)$, and $d^{FF} = 4.1(9)$. A study of molecular magnetic effects has yielded the two molecular $g$-factors $g_\perp = -0.04460(4)$ nm and $g_\parallel = -0.03370(30)$ nm as well as the anisotropy in the susceptibility $(\chi_\parallel - \chi_\perp) = -28(5) \times 10^{-30}$ J/T$^2$. The molecular quadrupole moment has been calculated. From a study of the Stark effect, the electric dipole moment has been determined for the ground vibrational state and for the ($v_5 = 1$) and ($v_6 = 1$) fundamentals. The results are: $\mu = 1.86847(10)$ D, $(\mu_5 - \mu)/\mu = -3.49(4) \times 10^{-3}$, and $(\mu_6 - \mu)/\mu = -0.65(4) \times 10^{-3}$. For each of these two excited vibrational states, the $l$-doubling constants $q_t$ and $D_{qJ}^{(t)}$ ($t = 5,6$) have been obtained. This work demonstrates that the molecular beam electric resonance method can be applied to symmetric tops with relatively large room temperature rotational partition functions by reducing the rotational temperature to a few degrees kelvin with the seeded beam technique.

Le spectre de résonance électrique d'un faisceau moléculaire de fluorure de phosphoryle ($^{16}OPF_3$) a été étudié. On a combiné l'analyse de la structure hyperfine de multiplets ($K = 0$) avec des données de résonance magnétique obtenues antérieurement et avec des arguments chimiques pour obtenir quatre constantes spin–rotation et deux constantes tensorielles spin–spin. Les résultats (en kHz) sont les suivants: $C_\perp^P = +7.7(8)$, $C_\parallel^P = +21(6)$, $C_\perp^F = +4.6(4)$, $C_\parallel^F = +4.0(2.5)$, $d^{PF} = 2.3(9)$ et $d^{FF} = 4.1(9)$. Une étude des effets magnétiques moléculaires a donné les deux facteurs $g$ moléculaires $g_\perp = -0.04460(4)$ nm et $g_\parallel = -0.03370(30)$ nm, ainsi que l'anisotropie dans la susceptibilité $(\chi_\parallel - \chi_\perp) = -28(5) \times 10^{-30}$ J/T$^2$. Le moment de quadrupole de la molécule a été calculé. A partir d'une étude de l'effet Stark, le moment de dipole eléctrique a été déterminé pour l'état fondamental de vibration et les fondamentales ($v_5 = 1$) et ($v_6 = 1$). Les résultats sont les suivants: $\mu = 1.86847(10)$ D, $(\mu_5 = \mu)/\mu = -3.49(4) \times 10^{-3}$ et $(\mu_6 - \mu)/\mu = -0.65(4) \times 10^{-3}$. Pour chacun de ces deux états vibrationnels excités, les constantes de doublage $l$ $q_t$ et $D_{qJ}^{(t)}$ ($t = 5,6$) ont été obtenues. Ce travail démontre que la méthode de résonance électrique de faisceau moléculaire peut être appliquée à des toupies symétriques ayant une fonction de partition pour les états de rotation relativement grande à la température ambiante, en utilisant une technique qui permet d'abaisser la température rotationnelle à quelques degrés kelvin.

[Traduit par le journal]

Can. J. Phys., 57, 1163 (1979)

## 1. Introduction

In the past, the study of symmetric rotors with the molecular beam electric resonance (MBER) method has been restricted to molecules such as $CH_3D$ (1), $CH_3F$ (2), and $PH_3$ (3) which have relatively large rotational constants. One of the major problems in applying this method to molecules with smaller rotational constants has been the low fractional population that is obtained in the individual rotation states with an effusive source. With the development of nozzle source techniques (4), it has become possible to overcome this difficulty. The rotational temperature of the molecules in the beam can be reduced dramatically while at the same time substantially increasing the total beam intensity in the forward direction. Successful use has been made of this technique in several beam maser studies of symmetric tops (5–7). The cooling effect can be further enhanced (8, 9) by using a 'seeded' beam formed by passing through the supersonic nozzle a mixture consisting of a small percentage of the molecule under study with a noble gas.

The present work on phosphoryl fluoride ($OPF_3$) was undertaken to demonstrate the feasibility of the MBER method for the study of heavy symmetric top molecules, to study the hyperfine and molecular magnetic effects, and to obtain as complete a description as possible of the electric dipole moment. Following a general description of the experimental method, each of the four topics investigated is discussed in a separate section; the first three of these deal with the ground vibronic state. In Sect. 3 on hyperfine effects, the determination is described of the spin–rotation constants $c_\perp^P$, $c_\parallel^P$, $c_\perp^F$, and $c_\parallel^F$. Here the superscripts P and F refer to the phos-

[1]Permanent address: Department of Physics, University of British Columbia, Vancouver, B.C., Canada V6R 2A5.

0008-4204/79/081163-11$01.00/0

phorus and fluorine nuclei, respectively. The subscript $\|$ refers to the component about the symmetry axis while the subscript $\perp$ indicates that an average is to be taken for the components about the other two molecular axes. The magnitudes of $c_\perp{}^P$ and $c_\perp{}^F$ were determined experimentally, as well as their relative sign. By using earlier molecular beam magnetic resonance (MBMR) data (10) and the relationship between the spin–rotation and nuclear shielding tensors (11), the magnitudes and absolute signs of all four constants were obtained. In addition, the phosphorus–fluorine and fluorine–fluorine dipole–dipole constants $d^{PF}$ and $d^{FF}$, respectively, were measured. In Sect. 4, the determination of the permanent electric dipole moment $\mu$ is presented. In the Appendix, the usual expansion for the Stark energy as a power series in the electric field $\varepsilon$ is extended to include terms in $\mu^3$ and in the anisotropy in the polarizability. In Sect. 5 on molecular magnetic effects, the measurement is described of the two molecular $g$-factors $g_\|$ and $g_\perp$, and of the anisotropy $(\chi_\| - \chi_\perp)$ in the magnetic susceptibility tensor. The absolute sign of the $g$-factors was determined by the avoided crossing method (12). The molecular quadrupole moment $\theta_\|$ was calculated from the molecular $g$-factors and $(\chi_\| - \chi_\perp)$. In Sect. 6, the electric dipole moment was measured in each of the two lowest lying triply degenerate states, namely $(v_5 = 1)$ and $(v_6 = 1)$. In addition, the $l$-doublet splittings in these states were studied. The results obtained here for the ground vibronic state are summarized in Table 1.

Four closely related studies of $OPF_3$ have been reported recently. First, an avoided crossing method (12) has been developed which permits the direct measurement of the rotational constants $A_0$ about the symmetry axis and a detailed study of the effects of centrifugal distortion on $\mu$. The development of this new method provided the motivation for selecting $OPF_3$ for the current work. Second, the normal millimetre wave spectrum has been examined (13) in great detail for the ground vibrational state as well as for several excited states. Third, the distortion dipole microwave spectrum obeying the selection rules $(\Delta J = 0, \Delta K = \pm 3)$ has been reported for the ground vibrational state (14). Finally, laser Stark spectroscopy has been used to study the $(v_4 = 1)$ vibrational level (15).

## 2. General Experimental Method

The basic MBER apparatus used has been described in detail elsewhere (16). To obtain the very low rotational temperatures required, the seeded beam technique was used; a mixture of 4% $OPF_3$ in argon was passed through a 20 μm nozzle at a backing pressure of 0.75 bar. Commercial gases were used and the $OPF_3$ beam was monitored at the ion peak $m/e = 85$. Except for some of the excited state work, the source itself was maintained at room temperature.

The velocity distribution in the beam was investigated. It was found that the most probable velocity in the beam $v_p = 550$ m/s while the full width at half height of the distribution $\Delta v = 0.09 v_p$. These results allow us to correct for the translational Stark effect in the measurement of $(\chi_\| - \chi_\perp)$ as described in Sect. 5 and to determine the instrumental line width for the hyperfine studies described in Sect. 3. Furthermore, these velocity measurements provide valuable insight into the internal temperature of the $OPF_3$ molecules in the beam. Using methods developed for OCS (9), it was shown that the $OPF_3$ speed ratio is 18(2) and the translational temperature is 6(1) K. By analogy with the OCS studies (9), it is expected that this translational measurement in the $OPF_3$ beam is a good approximation to the rotational temperature. No detailed quantitative intensity measurements were made on the MBER spectrum of $OPF_3$ to check this result. However, a qualitative comparison of the relative intensities of the spectra studied here and in ref. 12, which together sample a

TABLE 1. Hyperfine constants, magnetic constants, and electric dipole moment of $OPF_3$ in the ground vibrational state

| Quantity | Present work[a] | Other values |
|---|---|---|
| $c_\perp{}^P$ (kHz) | 7.7(8)[b] | |
| $c_\perp{}^F$ (kHz) | 4.6(4)[b] | |
| $d^{PF}$ (kHz) | −2.3(9) | −2.51[c] |
| $d^{FF}$ (kHz) | 4.1(9) | 4.095[c] |
| $c_a{}^P$ (kHz) | | 12(2)[d] |
| $c_a{}^F$ (kHz) | | 4.4(8)[d] |
| $c_\|{}^P$ (kHz) | 21(6)[e] | |
| $c_\|{}^F$ (kHz) | 4.0(2.5)[e] | |
| $\mu$ (D) | 1.86847(10) | 1.86952(40)[f] |
| $g_\perp$ (nm) | −0.04460(4)[i] | 0.0440(5)[g] |
| $g_\|$ (nm) | −0.03370(30)[i] | |
| $(\chi_\| - \chi_\perp)$ $(10^{-30}$ J/T$^2)$[j] | −28(5) | −30(13)[h] |
| $\theta_\|$ $(10^{-39}$ C m$^2)$[k] | −1.53(11) | |

[a] The value obtained for the linewidth $\Delta\nu_L$ from the hyperfine analysis was 3.6(6) kHz.
[b] The magnitudes and relative sign of $c_\perp{}^P$ and $c_\perp{}^F$ were obtained from the hyperfine analysis. The determination of the absolute sign required use of MBMR data (10) and shielding arguments.
[c] These are classical values calculated from the structure (13, 14).
[d] The magnitudes of $c_a{}^P$ and $c_a{}^F$ are from MBMR data (10). The determination of the signs is based on shielding arguments given here.
[e] $c_\|$ is derived from $c_a$ and $c_\perp$.
[f] This is the value from ref. 15 after being corrected as described in Sect. 4.
[g] The magnitude was determined experimentally in ref. 35. The sign was deduced as negative in ref. 35 from theoretical arguments based on the magnitude of $\theta_\|$ which in turn was determined from an assumed value for $|g_\||$ that is in error by a factor of over two. This sign determination is not considered to be reliable and so is not shown in the body of the table.
[h] Reference 35.
[i] The sign was taken from ref. 12.
[j] $(10^{-30}$ J/T$^2) = 0.0602205\ (10^{-6}$ erg G$^{-2}$ mol$^{-1})$.
[k] $(10^{-39}$ C m$^2) = 2.9979\ (10^{-26}$ esu cm$^2)$.

great many transitions with $J$ in the range from 1 to 8, provides strong evidence that the rotational temperature is indeed very close to 6 K.

### 3. Hyperfine Structure

For a symmetric top in an external electric field $\boldsymbol{\varepsilon}$ and an external magnetic field $\boldsymbol{B}$, the effective Hamiltonian for problems within one rotational state can be formally written as:

$$[1] \quad H = H_{HYP} + H_{ST} + H_Z$$

Here, $H_{HYP}$ includes all the nuclear hyperfine interactions, while $H_{ST}$ and $H_Z$ represent the Stark and Zeeman Hamiltonians, respectively.

In the current work, $\varepsilon$ is selected so that the Stark energy is orders of magnitude larger than the other terms. In this case it is convenient to use the high field representation (1) characterized by the quantum numbers ($J$, $K$, $m_J$; $I_P$, $m_P$; $I_F$, $m_F$). The phosphorus nuclear spin $I_P = 1/2$. The fluorine nuclear spin $I_F = 3/2$ or $1/2$. Because of the $C_{3v}$ symmetry of $OPF_3$, the quantum number $K$ for the projection of the rotational angular momentum $\boldsymbol{J}$ on the symmetry axis must equal $3N$ ($N$ = integer) if $I_F = 3/2$; similarly $K \neq 3N$ if $I_F = 1/2$. If $\boldsymbol{\varepsilon}$ and $\boldsymbol{B}$ are parallel as is the case here, then $m_J$, $m_P$, and $m_F$ correspond to the projections of $\boldsymbol{J}$, $\boldsymbol{I}_P$, and $\boldsymbol{I}_F$, respectively, along the common external field direction. The large value of $\varepsilon$ makes $m_J$ a good quantum number, but this is not sufficient for $m_P$ and $m_F$ because $H_{HYP}$ has off-diagonal matrix elements of the type $\Delta m_J = 0$, $\Delta m_P = \pm 1$, $\Delta m_F = \mp 1$. To make $m_P$ and $m_F$ good quantum numbers, the Zeeman energy $E_Z$ must introduce a splitting between connected levels that is large compared to the mixing terms. Because the nuclear Zeeman effect is large, a value of $\boldsymbol{B} \sim 2$ mT (20 G) is adequate.

The selection rules for the transitions studied are $\Delta m_J = \pm 1$, $\Delta J = \Delta K = \Delta m_P = \Delta m_F = 0$. Such transitions $(J_{\pm|K|}, \mp|m_J| \rightarrow (J_{\pm|K|}, \mp(|m_J| - 1))$ abbreviated as $(J_{\pm|K|}, \mp|m_J| \rightarrow \mp(|m_J| - 1))$ can be labelled by $(\Delta m_J, m_P, m_F)$; herein $\Delta m_J = +1$ and $\Delta m_J = -1$ indicate the upper and lower signs, respectively.[2]

Under the conditions used here, the hyperfine energy $E_{HYP}$ will be closely approximated by the diagonal matrix elements of $H_{HYP}$ in the high-field representation (1, 3, 7):

$$[2] \quad \langle H_{HYP} \rangle = m_P m_J \left[ c_\perp^P + \frac{K^2}{J(J+1)} (c_\parallel^P - c_\perp^P) \right] + m_F m_J \left[ c_\perp^F + \frac{K^2}{J(J+1)} (c_\parallel^F - c_\perp^F) \right]$$
$$+ \frac{2I_F[3m_F^2 - I_F(I_F+1)][3K^2 - J(J+1)][3m_J^2 - J(J+1)]}{3(2I_F - 1)J(J+1)(2J-1)(2J+3)} \delta_{K,3N} d^{FF}$$
$$- d^{PF} \frac{2m_P m_F[3K^2 - J(J+1)][3m_J^2 - J(J+1)]}{J(J+1)(2J-1)(2J+3)}$$

The first two terms arise in turn from the phosphorus and fluorine spin–rotation interactions. The associated constants were introduced in Sect. 1; they are related to those of Wofsy *et al.* (1) by $c_\perp^P = -c_\alpha$, $c_\parallel^P = -c_\beta$, $c_\perp^F = -\zeta_\alpha$, and $c_\parallel^F = -\zeta_\beta$. The sign convention used here is the reverse of that used in the MBMR literature (17). The third and fourth terms in [2] arise, respectively, from the fluorine–fluorine and phosphorus–fluorine tensor dipole–dipole interactions. In SI units,

$$d^{FF} = \mu_0 \mu_N^2 g_F^2 / 8\pi R_{FF}^3$$

$$[3] \quad d^{PF} = \frac{\mu_0 \mu_N^2 g_P g_F}{4\pi R_{PF}^3} [1 - \tfrac{3}{2} \sin^2 \theta_0]$$

Here $R_{FF}$ and $R_{PF}$ are the fluorine–fluorine and fluorine–phosphorus bond lengths, respectively; $\theta_0$ is the angle between the O—P and P—F bonds and $g_F$ and $g_P$ are the fluorine and phosphorus $g$-factors, respectively; $\mu_0$ is the permeability of vacuum and $\mu_N$ is the nuclear magneton. The electron-coupled spin–spin interactions have been omitted here (see below). The $K$-doubling terms (1) that enter for $K = \pm 1$ have been omitted because these values of $K$ do not enter the present study. The Stark energy $E_{ST}$ is discussed in Sect. 4 and in the Appendix. The Zeeman energy $E_Z$ is discussed in Sect. 5.

Measurement of the various constants entering $H$ is considerably complicated by the fact that the hyperfine effects are so small compared to the instrumental resolution that it is impossible to obtain fully resolved spectra. In order to simplify the problem, it is necessary to make $\varepsilon$ large enough that the second-order Stark effect separates the spectrum into different multiplets, each labelled by its values

[2] It should be noted that the energy differences between the final and initial states are positive and negative for states with $K = 0$ and $K \neq 0$, respectively.

of $(J_K, m_J \rightarrow m_J')$. The hyperfine contribution to the frequency can be calculated approximately from [2]. The Stark contribution (see Appendix) will only shift the pattern as a whole. The Zeeman contribution (see Sect. 5) introduces a splitting which depends to first approximation only on the molecular $g$-factors because $\Delta m_P = \Delta m_F = 0$. For $B \sim 2$ mT, this splitting appears only as a small symmetric broadening which can easily be taken into account. Thus the multiplet pattern depends only on the hyperfine constants.

Detailed hyperfine studies could be made only for states with $K = 0$. For the large values of $\varepsilon$ required to separate the multiplets sufficiently from one another, the states with $K \neq 0$ had Stark shifts $\sim 100$ MHz and inhomogeneity broadening $\sim 5$ kHz. The full width $\Delta\nu_L$ at half height of the instrumental line shape in the absence of inhomogeneity broadening was 3.6 kHz (see below). Because of the large resulting total line width, the small hyperfine splittings could not be resolved and each $(K \neq 0)$ multiplet investigated appeared as a broad structureless feature with widths of 12 to 20 kHz. (The specific cases examined are listed in Table 2 in Sect. 5.) However, for $K = 0$, there is only a quadratic Stark effect and the inhomogeneity broadening is negligible. For each $(K = 0)$ multiplet investigated, a partially resolved hyperfine pattern was observed. The specific cases examined were $(J_K = 1_0, m_J = \mp 1 \rightarrow 0)$, $(2_0, \mp 2 \rightarrow \mp 1)$, $(2_0, \mp 1 \rightarrow 0)$, $(3_0, \mp 1 \rightarrow 0)$, and $(4_0, \mp 2 \rightarrow \mp 1)$. For the first three cases, detailed studies were made; the observed spectra are shown in Fig.1.

To extract the hyperfine constants, a theoretical spectrum was generated and compared to the experimental data. Each multiplet consisted of 16 lines corresponding to the different possible values of $(\Delta m_J, m_P, m_F)$. These lines fell in pairs $(+1, m_P, m_F)$ and $(-1, -m_P, -m_F)$ split only by the small molecular Zeeman effect. To obtain the frequency of each line, the Stark energy was taken from the second (see Appendix) and fourth order expressions (18) resulting from $\mu$. The contribution due to the anisotropy $(\alpha_{\parallel} - \alpha_{\perp})$ in the polarizability was negligible. For each $J_K$, the Hamiltonian $H$ including all matrix elements off-diagonal in $m_J$, $m_P$, and $m_F$ (1, 3, 7) was diagonalized. Once the frequencies were calculated, each transition was assigned unit weight and the monovelocity molecular beam lineshape (17) was assumed. The 16 lines were then added and the resulting curve was renormalized so that the area matched that for the experimental multiplet.

The theoretical intensity $I_T$ and experimental intensity $I_E$ were then compared using the method of ref. 19. The variance which characterizes the overall quality of the fit is:

$$[4] \quad \sigma^2 = \left(\frac{1}{N}\right) \sum_{i,n} [I_T''(i) - I_E''(i)]^2$$

where $n = 1, 2, 3$ labels the three multiplets studied and $i = 1, 2 \ldots, 500$ labels the point at which the individual multiplets were digitized; $N$ is the number of degrees of freedom:

$$[5] \quad N \simeq (\Delta\nu_T/\Delta\nu_L) - N_P$$

where $\Delta\nu_T$ is the combined frequency interval (110 kHz) digitized for the three multiplets and $N_P$ is the number of parameters varied in the fit. Since $\Delta\nu_L = 3.6$ kHz and $N_P = 5$ in the final fit, $N = 26$, a value which is large enough that the approximation in [5] is adequate.

The best values $\{\bar{c}_j\}$ $(j = 1, 2, \ldots, N_P)$ of the adjustable parameters $\{c_j\}$ are obtained by varying the $\{c_j\}$ until $\sigma^2$ attains its minimum value $\sigma_m^2$. The errors $\{\Delta c_j\}$ in the $\{\bar{c}_j\}$ are obtained by applying an $F$-test to the ratio $F \equiv \sigma^2/\sigma_m^2$. To calculate a specific $\Delta c_k$, $c_k$ is fixed at $\bar{c}_k + \varepsilon(k)$ where $\varepsilon(k)$ is some small increase in $c_k$ and the remaining parameters are varied to find the minimum value $\sigma_{\varepsilon(k)}^2$ of $\sigma^2$; $\varepsilon(k)$ is varied until $(\sigma_{\varepsilon(k)}/\sigma_m^2)$ equals the $F$-value (1.94) appropriate to the number of degrees of freedom (26) and the confidence level selected (95%). The magnitude of the resulting value of $\varepsilon(k)$ is then averaged with the corresponding magnitude obtained when $\varepsilon(k)$ is taken as a small decrease in $c_k$ to give the final error $\Delta c_k$. For all the fits here, $\sigma^2$ was parabolic in shape and the two magnitudes did not differ significantly. The errors $\{\Delta c_j\}$ obtained in this way take into account correlation effects between parameters.

The shape of the $(K = 0)$ hyperfine multiplets is sensitive to four molecular constants: $c_\perp^P$, $c_\perp^F$, $d^{PF}$, and $d^{FF}$, as well as to one apparatus parameter: $\Delta\nu_L$. Only one line width was required because each of the three multiplets was observed at its own value for the rf electric field at which the transition probability was optimal (17). All five parameters were allowed to vary; the best values and the corresponding errors are given in Table 1. The value of $\Delta\nu_L$ is very close to that expected from the time-of-flight through the transition region. If the electron-coupled contribution to $d^{PF}$ and $d^{FF}$ is neglected, these constants can be calculated from the molecular geometry (13, 14). As can be seen from Table 1, these classical values agree well with those obtained from the fit. As a check, $d^{PF}$ and $d^{FF}$ were fixed at the classical values and $c_\perp^P$, $c_\perp^F$, and $\Delta\nu_L$ were varied in a second fit. The results obtained agreed with those given in Table 1 to well within the errors. The agreement was expected *a priori*, because the correlations in the five

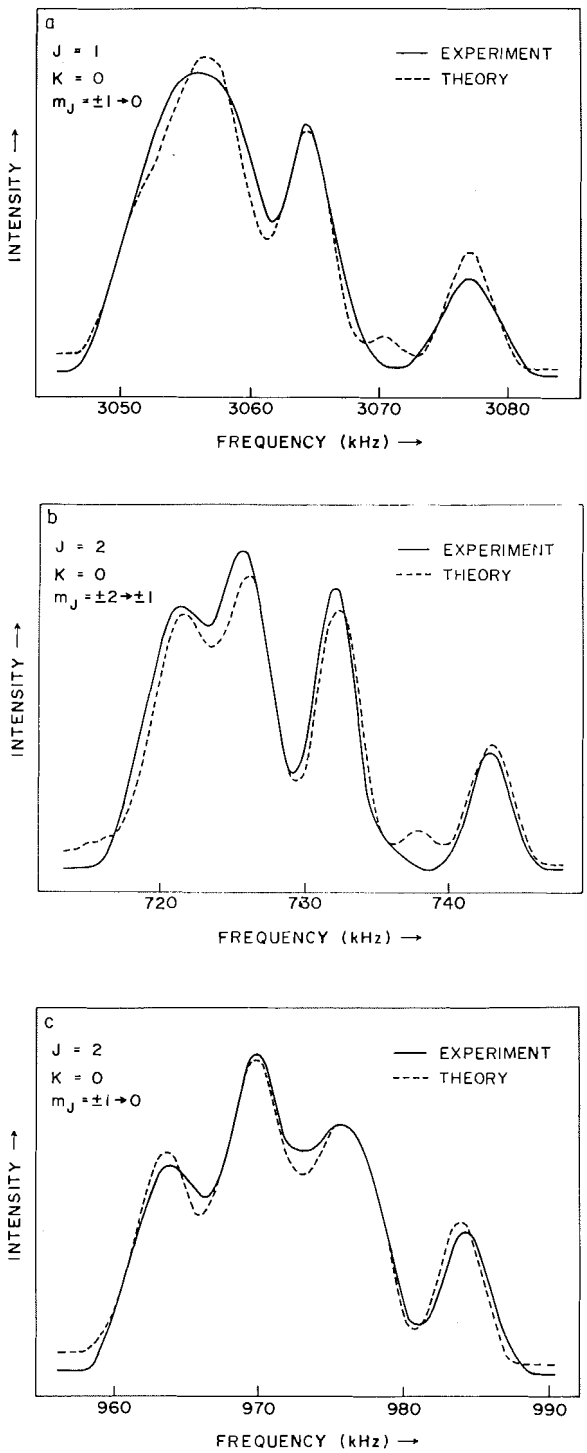


FIG. 1. The three multiplets used in the detailed hyperfine studies. Each experimental curve is the smoothed average of one sweep up and one down. For a time constant of 3 s, the signal-to-noise was typically 20. The electric fields used were (in V/cm): (*a*) and (*b*) 325.482; (*c*) 650.960. The magnetic fields used were (in mT): (*a*) 2.16; (*b*) and (*c*) 1.57.

parameter fits were small. The agreement between the spectra calculated for $\{\bar{c}_j\}$ and the experimental curves is good, as can be seen from Fig. 1.

The success of this curve-fitting procedure depends on the fact that $m_P$ and $m_F$ are good quantum numbers. When $\boldsymbol{I}_P$ and $\boldsymbol{I}_F$ are uncoupled, all 16 lines in a given multiplet have the same transition moment. As a result, all 16 have the *same intensity* and the same line width $\Delta\nu_L$. This line width cannot be calculated *a priori* for ($\Delta m_J = \pm 1$) transitions because it depends on the angle between the rf and static electric fields, but we can overcome this problem by introducing $\Delta\nu_L$ as a fitting parameter. If each multiplet is run at its own optimum rf perturbation, only a single line width enters the entire fit. In the end, the results are only moderately sensitive to $\Delta\nu_L$. On the other hand, if $B = 0$ so that $\boldsymbol{I}_P$ and $\boldsymbol{I}_F$ are coupled, the various lines in an individual multiplet have different transition moments. The single lines then have different relative intensities and linewidths. The resulting lineshape calculation then becomes intractable.

To this point, the magnitudes of $c_\perp^F$ and $c_\perp^P$ have been measured and it has also been found from the fit of the spectra that the two constants have the same sign. A complete determination of the absolute signs and magnitudes of all four spin–rotation constants in [2] can be made by combining the present measurements with MBMR results and using the relationship between the spin–rotation interaction and the nuclear shielding (17, 20, 11, 21). Both the phosphorus and fluorine MBMR spectra have been studied (10). For each nucleus, $c_\perp$ and $c_\parallel$ were very strongly correlated and only the average spin–rotation constant $c_a \equiv 1/3(2c_\perp + c_\parallel)$ was well determined. The magnitudes of $c_a^F$ and $c_a^P$ are given in Table I; the spectra contain no sign information.

To determine the sign of $c_a$ for each nucleus, we introduce the modified paramagnetic shielding $\sigma_P'$ (11). In a symmetric top,

$$[6] \quad \sigma_P' = -\frac{M}{6mg_\lambda}\left[\frac{2c_\perp^\lambda}{B_0} + \frac{c_\parallel^\lambda}{A_0}\right]$$

where $M$ and $m$ are the proton and electron masses, respectively, and $g_\lambda$ is the nuclear $g$-factor of the $\lambda$ nucleus ($\lambda \equiv$ P or F); $A_0$ and $B_0$ are the rotational constants parallel and perpendicular to the symmetry axis, respectively. For a linear molecule the second term in [6] vanishes: For $OPF_3$, $(A_0 - B_0)/B_0$ is very small, so that

$$[7] \quad \sigma_P' \simeq -\frac{M}{2mg_\lambda}\frac{c_a^\lambda}{B_a}$$

where $B_a \simeq 1/2(A_0 + B_0) = 4703$ MHz (14). The

change $\Delta\sigma_P'$ from $OPF_3$ to an appropriate reference molecule should approximate the corresponding chemical shift $\Delta\sigma$ and so can be used to fix the sign of $c_a$. For the fluorine nucleus, the reference selected was $F_2$, for which both $c$ (22) and $B_0$ (23) are well known. For $c_a^F > 0$, $\Delta\sigma_P' = 529(30)$ ppm and for $c_a^F < 0$, $\Delta\sigma_P' = 856(30)$ ppm. Since $\Delta\sigma = 523$ ppm (24), it is clear $c_a^F > 0$. For the phosphorus nucleus, the reference selected was $PH_3$, for which the spin–rotation constants (3) and rotational constants (25) are also well known. For $c_a^P > 0$, $\Delta\sigma_P' = -670(180)$ ppm and for $c_a^P < 0$, $\Delta\sigma_P' = +1400(180)$ ppm. Since $\Delta\sigma = -203$ ppm (26), it is clear $c_a^P > 0$ as well, in spite of the fact that the match in this case is not as good as in the fluorine case. For each nucleus, the errors given in $\Delta\sigma_P'$ are entirely due to the error in $|c_a|$.

Thus far, there has been presented the determination of the magnitudes and signs of $c_a^F$ and $c_a^P$ as well as the magnitudes and relative sign of $c_\perp^F$ and $c_\perp^P$. To complete the problem, the theoretical spectrum for the ($J_K = 3_{\pm 3}$, $m_J = \mp 2 \rightarrow \mp 1$) multiplet was calculated first for both $c_\perp^F$ and $c_\perp^P$ positive and then for both negative. Because $K \neq 0$, the instrumental lineshape was modified to take approximate account of the inhomogeneity broadening present under the experimental conditions. For $c_\perp^F$ and $c_\perp^P$ both negative, the calculated spectrum showed well-resolved structure extending over $\sim 80$ kHz. For both constants positive, the calculated spectrum was confined to a 40 kHz range and showed no clear structure. The expected full width at half height was 20 to 25 kHz. The experimental curve consisted of a single peak 20 kHz wide. This clearly demonstrates that the positive sign is correct. This was confirmed with calculations on the other ($K \neq 0$) multiplets observed. The values of $c_\parallel^F$ and $c_\parallel^P$ corresponding to the positive signs are given in Table 1.

A comment should be made regarding the role of the electron-coupled spin–spin (ECSS) interactions in the current work. In the high resolution nmr literature (24, 26), the scalar and tensor ECSS phosphorus–fluorine constants are denoted $J_{PF}$ and $\Delta J_{PF}$, respectively. The fluorine–fluorine constants should be negligible because these atoms are not directly bonded. $J_{PF} = -1.0720(8)$ kHz (in $Cl_4$ solution) (27) is large enough that some significant effect on the spectrum might be expected. However, because $\Delta m_P = \Delta m_F = 0$, this constant does not contribute to the frequencies. The effect of $\Delta J_{PF}$ does not vanish; it enters (27) by adding a term $[-\Delta J_{PF}/3]$ to the classical definition of $d^{PF}$ given in [3]. Liquid crystal studies (27) have been interpreted by fixing $\Delta J_{PF}$ at zero and by allowing it to vary. In the latter case, it was found that $[-\Delta J_{PF}/3] \sim 0.9$ kHz. Both interpretations are consistent with the current data because (see Table 1) $d^{PF}$(observed) $-$ $d^{PF}$(classical) $= (0.2 \pm 0.9)$ kHz.

## 4. The Ground State Electric Dipole Moment

A precision measurement of the dipole moment in the ground vibrational state was carried out because there is considerable interest in the variation of the moment with vibrational and rotational state, and because this molecule is the prototype for the avoided crossing technique recently developed (12). The experimental requirements here are quite different from those in the hyperfine study in Sect. 3 because we are now concerned with the central frequency of the multiplet pattern rather than its structure. Again the electric field $\varepsilon$ was set to values large enough that the quadratic Stark effect separated the different multiplets, but now the ($K \neq 0$) transitions were selected. Under the conditions used, the typical multiplet with a linear Stark effect appeared as a single broad structureless feature centered at $\gtrsim 100$ MHz with a width $\sim 20$ kHz determined primarily by hyperfine effects and field inhomogeneity of $\sim 5$ parts in $10^5$. Both of these contributions to the width can in general introduce shifts. However, for the large Stark splittings occurring here, these shifts are negligible.

The Stark effect of interest is generated by the electric dipole moment along the symmetry axis and by the anisotropy $(\alpha_\parallel - \alpha_\perp)$ in the polarizability tensor $\boldsymbol{\alpha}$. The distortion dipole moment $\mu_D$ perpendicular to the axis is neglected because it has significant effects only near avoided crossings, regions which do not enter in this study. The contribution of the trace of $\boldsymbol{\alpha}$ is independent of the molecular orientation and so does not affect the frequencies. Because the Stark effect is much smaller than the splittings between levels mixed by $\boldsymbol{\mu}$ or $\boldsymbol{\alpha}$, the Stark energy $E_{ST}$ can be expressed as a power series in $\varepsilon$. General expressions for the linear and quadratic terms in $\mu$ are available in the literature (28), but those quadratic in $\varepsilon$ due to $(\alpha_\parallel - \alpha_\perp)$ and cubic in $\varepsilon$ due to $\mu$ are not. They have been calculated here using standard perturbation techniques and are given in the Appendix. For completeness, the lower order terms are listed as well. These expressions should be useful in a variety of applications. They were essential for search purposes and preliminary interpretation of data both here and in ref. 12. In the final data analysis, the rotational and Stark matrices were diagonalized after truncation at $\Delta J \leq 3$. The rotational constants necessary are known very accurately (13, 14). The differences between the results of the diagonalization and those of the perturbation cal-

culation were in the order of the experimental errors.

The electric dipole moment was first determined from the ($J_K = 3_{\pm 2}$, $m_J = \mp 1 \rightarrow 0$) multiplet. The $3_2$ case was selected because the term in $(\alpha_\parallel - \alpha_\perp)$ vanishes (see Appendix) and because the hyperfine energy reduces to $c_a^{\mathrm{P}} m_J m_{\mathrm{P}} + c_a^{\mathrm{F}} m_J m_{\mathrm{F}}$. As a result, the multiplet is symmetric about a frequency determined entirely by $\mu$ (and rotational constants). As a check, a second measurement was made from the ($2_{\pm 1}$, $m_J = \mp 1 \rightarrow 0$) multiplet. Here the contribution of the anisotropy in the polarizability is not zero, but is negligible for any physically reasonable value of $(\alpha_\parallel - \alpha_\perp)$.

The values of $\mu$ obtained are 1.868465(20) D for the $3_{\pm 2}$ state and 1.868475(40) D for the $2_{\pm 1}$ state. The errors reflect only those which enter relative measurements, namely the statistical uncertainty in the frequency measurement and, for the $2_{\pm 1}$ case, an upper limit to the hyperfine shift. The value of $\mu$ will depend on $J_K$ (12):

$$[8] \quad \mu(J, K) = \mu_0 - J(J+1)\mu_J - K^2\mu_K$$

where $\mu_K$ and $\mu_J$ are dipole distortion constants. The value of $\mu_J$ is given in Sect. 6 (see Table 5) and $\mu_K$ can be expected to have the same order of magnitude. It follows then that the expected difference $|\mu(3, \pm 2) - \mu(2, \pm 1)|$ will be $\sim 2 \times 10^{-5}$ D and the two measurements of $\mu$ can be expected to agree within the error of $4.5 \times 10^{-5}$ D. The actual values do agree to well within this error; the internal consistency is excellent.

The final value of $\mu$ is given in Table 1. The error listed is that for the absolute measurement and is dominated by the field calibration which was done using OCS in its ground vibrational state. No calibration procedure of higher accuracy is currently available. The value taken for $\mu$(OCS) was 0.71519(3) D (29) and the fundamental constants were taken from Cohen and Taylor (30). Because the absolute error is $10 \times 10^{-5}$ D, the value listed can be taken to be $\mu_0$ in [8].

The electric dipole moment of $OPF_3$ has recently been measured using laser Stark spectroscopy (15). The result obtained has been corrected to the values $\mu$(OCS) and $h$ used here and is listed in Table 1. The difference from the current measurement is $(100 \pm 40) \times 10^{-5}$ D, where the error is dominated by the uncertainty in the laser Stark determination. This difference is too large to be accounted for by $\mu_J$ and $\mu_K$. The experimental error quoted in ref. 15 was the estimated uncertainty in the calibration of the electrode spacing in the Stark cell. Because this is a very complex procedure (31), it is felt that this calibration may be the source of the difference.

## 5. The Molecular Zeeman Effect

For the transitions obeying the selection rules $\Delta m_J = \pm 1$, $\Delta m_{\mathrm{P}} = \Delta m_{\mathrm{F}} = 0$, the magnetic contribution to the frequencies can be calculated from those terms in the Zeeman energy which depend on $m_J$ (32, 7):

$$[9] \quad E_Z = -\mu_N B m_J \left[ g_\perp + (g_\parallel - g_\perp) \frac{K^2}{J(J+1)} \right] + \left[ \tfrac{2}{3}\mu_N B(\sigma_\parallel^{\mathrm{P}} - \sigma_\perp^{\mathrm{P}}) g_{\mathrm{P}} m_{\mathrm{P}} + \tfrac{2}{3}\mu_N B(\sigma_\parallel^{\mathrm{F}} - \sigma_\perp^{\mathrm{F}}) g_{\mathrm{F}} m_{\mathrm{F}} - \tfrac{1}{3}(\chi_\parallel - \chi_\perp) B^2 \right] \frac{[3K^2 - J(J+1)][3m_J^2 - J(J+1)]}{J(J+1)(2J-1)(2J+3)} + \mu_N B(\sigma_{aa}^{\mathrm{F}} - \sigma_{bb}^{\mathrm{F}}) g_{\mathrm{F}} m_{\mathrm{F}} \delta_{|K|,1} \times \frac{[3m_J^2 - J(J+1)]}{(2J+3)(2J-1)}$$

Here $(\sigma_\parallel^\lambda - \sigma_\perp^\lambda)$ is the shielding anisotropy for nucleus $\lambda$; $\sigma_{aa}^{\mathrm{F}}$ and $\sigma_{bb}^{\mathrm{F}}$ are the components of the fluorine shielding tensor along the two axes perpendicular to the symmetry axis (7). To [9] must be added a correction term (33) quadratic in both $B$ and the velocity $v$. This term arises from the translational Stark effect, that is from the interaction $-\boldsymbol{\mu} \cdot \boldsymbol{v} \times \boldsymbol{B}$ between the electric dipole moment and the motional electric field.

As mentioned in Sect. 3, each multiplet consists of 16 transitions for $K = 3N$ and 8 transitions otherwise. Lines with $(+1, m_{\mathrm{P}}, m_{\mathrm{F}})$ and $(-1, -m_{\mathrm{P}}, -m_{\mathrm{F}})$ denoted by $\nu_+$ and $\nu_-$, respectively, form pairs whose frequencies approach a common limit $\nu_0$ as $B$ goes to zero.[3] The splitting is proportional to $B$:

$$[10] \quad (\nu_+ - \nu_-) = -2\mu_N B g_{\mathrm{eff}}$$

Neglecting small corrections due to nuclear shielding effects,

$$[11] \quad g_{\mathrm{eff}} = [g_\perp + (g_\parallel - g_\perp)K^2/J(J+1)]$$

[3] Strictly speaking, $\nu_0 \equiv \frac{1}{2}(\nu_+ + \nu_-)$ for $B \sim 2$ mT, or alternatively, can be obtained by linear extrapolation to $B = 0$ of $\nu_+$ (or $\nu_-$) from the range 2 mT $\lesssim B \lesssim$ 10 mT. This care in the definition of $\nu_0$ is required by the fact that the high-field representation breaks down for $B \ll 2$ mT.

TABLE 2. Zeeman splittings and effective $g$-factors for ($K \neq 0$) multiplets

| Multiplet | | $\nu_0$ | $B$ | $\lvert\nu_+ - \nu_-\rvert$ | | |
|---|---|---|---|---|---|---|
| $J_K$ | $m_J \rightarrow m_J'$ | (MHz) | (T) | (kHz) | $g_{\text{eff}}$[a] (nm) | |
| $2_{\pm 1}$ | $\mp 1 \rightarrow 0$ | 124.253 | 0.64005 | 417.7(3.0) | $\frac{1}{6}g_\parallel + \frac{5}{6}g_\perp$ | −0.04280(31) |
| $3_{\pm 2}$ | $\mp 1 \rightarrow 0$ | 122.758 | 0.64005 | 400.6(2.0) | $\frac{1}{3}g_\parallel + \frac{2}{3}g_\perp$ | −0.04105(20) |
| $3_{\pm 3}$ | $\mp 2 \rightarrow \mp 1$ | 125.807 | 0.80037 | 443.7(3.0) | $\frac{3}{4}g_\parallel + \frac{1}{4}g_\perp$ | −0.03637(25) |

[a]The sign was taken from ref. 12.

Except for corrections due to the translational Stark effect, the shift $[\frac{1}{2}(\nu_+ + \nu_-) - \nu_0]$ of the average frequency from $\nu_0$ is determined by $(\chi_\parallel - \chi_\perp)$.

Both $g_\perp$ and $(\chi_\parallel - \chi_\perp)$ were measured using the $(1_0,\ m_J = \mp 1 \rightarrow 0)$ multiplet. This spectrum for $B \sim 2$ mT is shown in Fig. 1. The well-resolved feature at the high frequency end of the curve consists of the pair $(+1,\ m_P = 1/2,\ m_F = 3/2)$ and $(-1,\ -1/2,\ -3/2)$. For this particular pair:

$$[12]\quad g_{\text{eff}} = g_\perp - \tfrac{1}{5}g_P({\sigma_\parallel}^P - {\sigma_\perp}^P) - \tfrac{3}{5}g_F({\sigma_\parallel}^F - {\sigma_\perp}^F)$$

$$[13]\quad \tfrac{1}{2}(\nu_+ + \nu_-) - \nu_0 = -\tfrac{1}{5}(\chi_\parallel - \chi_\perp)B^2 + (vB/\varepsilon)^2\,\nu_0$$

Measurements were made at a series of magnetic fields between 0.2 and 0.8 T. $B$ was calibrated using $\Delta J = 0$, $m_J = \pm 1 \rightarrow 0$ transition of the $1_{11}$ state in $SO_2$ (34). The value of $g_\perp$ obtained is given in Table 1. The sign of $g_\perp$ (as well as $g_\parallel$) was taken from the avoided crossing work (12). The shielding corrections were made using the liquid crystal results (27); these corrections amounted to only 1 part in 2000. The value of $(\chi_\parallel - \chi_\perp)$ is also given in Table 1. The correction due to the translational Stark effect was done using the most probable velocity $v_P$ determined in Sect. 2; this correction amounted to about 10%.

The measurement of $g_\parallel$ was somewhat more difficult than that of $g_\perp$ because ($K \neq 0$) multiplets must be used and these show no hyperfine splittings. For each of three multiplets, the difference $(\nu_+ - \nu_-)$ was measured using the central frequencies of the patterns. The results are summarized in Table 2. Because the errors in $g_{\text{eff}}$ were larger, the shielding correction was omitted. The $J_K = 3_{\pm 2}$ state was studied because the hyperfine shifts vanish. In addition, $g_{\text{eff}}$ for this state is identically the average $g$-factor $g_a = 1/3(2g_\perp + g_\parallel)$. The $J_K = 3_{\pm 3}$ state was studied because its $g_{\text{eff}}$ receives the largest fractional contribution from $g_\parallel$ compared with the other states giving strong spectra. The final mean value for $g_\parallel$ is listed in Table 1.

The molecular quadrupole moment $\theta_\parallel$ can now be calculated from (32):

$$[14]\quad \theta_\parallel = \hbar\mu_N\left[\frac{g_\perp}{B_0} - \frac{g_\parallel}{A_0}\right] - \frac{4m}{e}(\chi_\parallel - \chi_\perp)$$

This calculation was carried out using the magnetic constants obtained here, and the rotational constants in the literature (13,14). The result is given in Table 1. The error is dominated by the contribution from $(\chi_\parallel - \chi_\perp)$. Since no *ab initio* calculations are available for $OPF_3$, the other derived quantities are not given here.

The current values for both $g_\perp$ and $(\chi_\parallel - \chi_\perp)$ agree well with the earlier, less accurate microwave results (35) as can be seen from the comparison in Table 1. No previous determination of $g_\parallel$ has been reported.

## 6. The ($v_5 = 1$) and ($v_6 = 1$) Excited Vibrational States

To characterize the energy levels of $OPF_3$ in a doubly degenerate fundamental vibrational state, it is necessary to modify the representation used. We introduce $l_t$ ($t = 4, 5, 6$) as the vibrational angular momentum quantum number: since $v_t = 1$, $l_t = \pm 1$. $\boldsymbol{J}$ is still the total angular momentum (exclusive of nuclear spin), but now contains a vibrational contribution. $K$ plays the same role with respect to $\boldsymbol{J}$ as it did in the ground state. A new basis is obtained by a Wang-type transformation:

$$[15]\quad |v_t, l_t, J, |K|, m_J, \pm\rangle = (1/\sqrt{2})\,\{|v_t, l_t, J, |K|, m_J\rangle \pm |v_t, -l_t, J, -|K|, m_J\rangle\}$$

Neither $K$ nor $l_t$ are individually good quantum numbers here, but $\overline{K} \equiv |K - l_t|$ is a good quantum number (36, 37).

For $\overline{K} = 0$ ($K = \pm 1$, $l_t = \pm 1$), the degeneracy between the $\pm$ levels is lifted in first order (38) by the $l$-doubling interaction denoted here by $H_q$:

$$[16]\quad \langle 1, 1, J, 1, m_J, \pm|H_q|1, 1, J, 1, m_J, \pm\rangle = \pm\tfrac{1}{2}J(J+1)[q_t - D_{qJ}{}^{(t)}J(J+1)]$$

$q_t$ is the $l$-doubling constant and $D_{qJ}{}^{(t)}$ is an empirical parameter introduced to allow for the expected

variation with $J$ of the effective $l$-doubling constant (36). In ref. 13, $q_t$ and $D_{qJ}^{(t)}$ are denoted $q_J^+$ and $q_J$, respectively. The general features of these degenerate vibrational states are very similar for $\overline{K} = 0$ to the features of the degenerate bending fundamental in a linear triatomic molecule and much of the analysis (39, 29) is identical in the two cases.

The transitions of interest here are those directly across the $l$-doublet between the $\pm$ levels indicated in [15]. Because the hyperfine energy is identical in these two states (29), here is no hyperfine contribution to the frequency. Thus in zero electric and magnetic field, the frequency depends only on $J$:

$$[17] \quad \nu_0^{(t)}(J) = q_t J(J+1) - D_{qJ}^{(t)} J^2 (J+1)^2 \qquad (t = 5, 6)$$

The $\pm$ levels have opposite parity and, in the presence of an electric field, repel one another through the Stark effect (39, 15):

$$[18] \quad \langle 1, 1, J, 1, m_J, \pm | (-\boldsymbol{\mu} \cdot \boldsymbol{\varepsilon}) | 1, 1, J, 1, m_J, \mp \rangle = -\mu\varepsilon m_J / J(J+1)$$

For each ($\Delta m_J = 0$) transition of interest here, the frequency can be calculated by solving the simple $2 \times 2$ matrix defined by [16] and [18]. The contributions quadratic in $\varepsilon$ from $\mu$ and $(\alpha_{\parallel} - \alpha_{\perp})$ cancel in this type of transition. Furthermore, the values of $\varepsilon$ have been chosen so that all higher order effects are negligible.

Zero-field $l$-doublet transitions have been observed for all $J$-values between 2 and 9 in the ($v_5 = 1$) and the ($v_6 = 1$) vibrational states. The identification was made using the values of $q_t$ ($t = 4, 5, 6$) given by Smith (13). The intensity of the transitions within the ($v_5 = 1$) state was increased by a factor $\sim$2.5 by operating the source at 175°C. The linewidth was 2 kHz for the room temperature work and somewhat larger when the source was heated. Typically, the signal-to-noise ratio for low $J$ was 5 for ($v_5 = 1$) with an effective time constant of 6 s and was 10 for ($v_6 = 1$) with an effective time constant of 3 s. The measured frequencies are given in Table 3.

For each of the two vibrational states, $q_t$ and $D_{qJ}^{(t)}$ were determined by a least-squares fit to the data; the values obtained are listed in Table 4. The differences between the observed and calculated frequencies are given in Table 3. The fit is clearly very good for both states.

It is known (37) that the ($\Delta l = 2$, $\Delta K = -1$) interaction associated with the coupling constant $r_t$ can affect the $l$-doublet splitting. A simple perturbation calculation shows that to lowest order the form of [17] is not changed; the $r_t$ contribution cannot be separated from the direct $l$-doubling contribution on the basis of the current data alone. The value of $r_t$ for $OPF_3$ is not known, but one would expect it to be considerably smaller than in $PF_3$ (36) and $CF_3H$ (37) where it is $\sim$1 MHz. For $r_t = 100$ kHz, the effect due to $r_t$ on the observed splittings is negligible. For $r_t = 1$ MHz, the contribution to $q_t$ is insignificant for $t = 5$ and marginally significant for $t = 6$; the contribution to $D_{qJ}^{(t)}$ is, however, $\sim$20% for both $t = 5$ and $t = 6$. The other known interactions that can in principle affect the $l$-doublet frequencies have a $J$ dependence that is of degree 6 or higher. These can be eliminated on the basis of the fact that the observed data do not have a significant term of degree higher than 4.

In Table 4, the current values for $q_t$ and $D_{qJ}^{(t)}$ ($t = 5, 6$) are compared to the earlier, less accurate millimetre wave values (13). The agreement is reasonable for ($v_6 = 1$) but there appears to be significant disagreement for ($v_5 = 1$), where $l$-resonance effects are known (13) to be large. The difficulty is believed to lie in the great complexity of the millimetre wave analysis, perhaps in correlations with constants that were of necessity fixed at zero. For example, the effective $l$-doubling constant (the square bracket in [16]) should contain a term $-D_{qK}^{(t)} \overline{K}^2$ when $\overline{K} \neq 0$ (36). This term was fixed at zero in the millimetre wave work, but may make a significant contribution. A reanalysis of the milli-

TABLE 3. Zero-field $l$-doubling transition frequencies for the ($v_5 = 1$) and ($v_6 = 1$) vibrational states

| $J_K$ | $\nu_0^{(5)a}$ | Deviation[b] | $\nu_0^{(6)a}$ | Deviation[b] |
|---|---|---|---|---|
| $2_1$ | 15 210.7(5) | 0.5 | 6 460.0(2) | 0.09 |
| $3_1$ | 30 418.0(10) | −0.1 | 12 922.2(2) | −0.01 |
| $4_1$ | 50 691.8(15) | 0 | 21 542.5(2) | 0.09 |
| $5_1$ | 76 025.3(20) | −2.8 | 32 323.7(2) | −0.03 |
| $6_1$ | 106 423.7(10) | 0.3 | 45 270.1(2) | 0.02 |
| $7_1$ | 141 873.2(20) | 0.2 | 60 386.2(2) | −0.07 |
| $8_1$ | 182 371.5(20) | 0.1 | 77 678.1(2) | −0.02 |
| $9_1$ | 227 912.2(30) | −0.4 | 97 151.8(2) | 0.03 |

[a]Observed frequency in kilohertz.
[b]Deviation (in kHz) ≡ observed frequency − calculated frequency obtained from [17] using the best fit constants given in Table 4.

TABLE 4. $l$-doubling constants in the ($v_5 = 1$) and ($v_6 = 1$) vibrational states

| Constant | Present work[a] (kHz) | Millimetre wave values[b] (kHz) |
|---|---|---|
| $q_5$ | 2535.226(43) | 2531.1(8) |
| $D_{qJ}^{(5)} \times 10^3$ | 31.8(8) | 17.6(4.2) |
| $q_6$ | 1076.4528(33) | 1075.8(6) |
| $D_{qJ}^{(6)} \times 10^3$ | −33.46(5) | −30.4(1.4) |

[a]The errors are based on a 95% confidence level.
[b]Reference 13.

TABLE 5. Electric dipole moments of $OPF_3$ in various vibrational states

| Quantity | Value | Reference |
|---|---|---|
| $\mu$ (D)[a] | 1.86847(10) | Present work |
| $\mu_J$ (D)[a] | $3.28(13) \times 10^{-6}$ | 12 |
| $\mu_D$ (D)[a] | $5.856(20) \times 10^{-6}$ | 12 |
| $(\mu_4 - \mu)/\mu$[b] | $-16.1(3) \times 10^{-3}$ | 15 |
| $(\mu_5 - \mu)/\mu$[b] | $-3.49(4) \times 10^{-3}$ | Present work |
| $(\mu_6 - \mu)/\mu$[b] | $-0.65(4) \times 10^{-3}$ | Present work |

[a]Ground vibrational state.
[b]$\mu_t$ is the dipole moment in the ($v_t = 1$) vibrational state ($t = 4, 5, 6$).

metre wave data with $q_5$ and $D_{qJ}^{(5)}$ fixed at the current values might clarify this point.

The electric dipole moment for each of these two vibrational levels has been determined from Stark shift measurements for $J_K = 2_1$ and $3_1$. For ($v_6 = 1$) each transition was measured for $\varepsilon = 61$ V/cm and for $\varepsilon = 118$ V/cm; for ($v_5 = 1$), only the higher field was used. For each vibrational level, the dipole moment obtained from the ($J_K = 2_1$) data agreed with that determined from the ($J_K = 3_2$) measurements to within the relative error of $\sim 2 \times 10^{-5}$. This indicates that accidental perturbations of the levels involved are not significant to this level of accuracy. The value of $\varepsilon$ was calibrated using the dipole moment of OCS in the ($J = 1$) state of the first excited bending vibrational level ($01^10$) (29). The Stark shifts were large enough that the errors in the absolute values of $\mu_t$ ($t = 5, 6$) were entirely determined by the uncertainty in $\varepsilon$. The error in the absolute value of the $OPF_3$ ground state moment was also dominated by its calibration (see Sect. 4), this time with the OCS ground state moment. Because the ratio of the OCS moments is known better than the individual absolute values (29), the ratios $\mu_t/\mu$ ($t = 5, 6$) are more accurately determined than the absolute values. Table 5 lists the results.

Table 5 summarizes all the data currently available on the dipole moment of $OPF_3$. Once $\mu_K$ is determined by extending the avoided crossing method (12), only the dipole moments for the three nondegenerate vibrations will be lacking from a complete description of the dipole moment of $^{16}OPF_3$. The possibility also exists of making similar measurements on the $^{17}O$ and $^{18}O$ modifications of $OPF_3$. It is hoped that the data in Table 5 and the potential extensions will stimulate a theoretical investigation of the dipole moment function of symmetric tops in general and of $OPF_3$ in particular.

## 7. Conclusion

In summary, it has been demonstrated that the MBER method can be applied to rather heavy symmetric rotors. The seeded beam method of lowering the rotational temperature successfully overcomes the problem of the large room temperature rotational partition function and the curve fitting procedure allows hyperfine studies to be made even when the coupling constants are only the order of a few kilohertz. For the ground vibrational state, molecular $g$-factors and anisotropy in the susceptibility have been obtained. In addition, the hyperfine constants have been determined by combining the present MBER data with earlier MBMR results and the relationship between the spin–rotation and shielding tensor. A precision study has been made of the electric dipole moment yielding $\mu$ for the ground state to 5 parts in $10^5$, as well as the ratios $\mu_5/\mu$ and $\mu_6/\mu$ for the vibrational states ($v_5 = 1$) and ($v_6 = 1$), respectively. An $l$-doubling study has been carried out for these two states. It is hoped that the current work will stimulate interest in the theoretical problem of how the electric dipole moment in a symmetric top changes with rotational and vibrational state.

## Acknowledgements

The authors wish to thank Dr. A. W. Ellenbroek for the use of his computer programs to calculate the hyperfine spectra and for many helpful discussions. One of us (I.O.) wishes to thank the National Research Council of Canada for its support through a travel grant covering the period when the experimental work was done. All three authors would like to thank the North Atlantic Treaty Organization Research Grant Programme for its support while the manuscript was being completed.

1. S. C. WOFSY, J. S. MUENTER, and W. KLEMPERER. J. Chem. Phys. **53**, 4005 (1970).
2. S. C. WOFSY, J. S. MUENTER, and W. KLEMPERER. J. Chem. Phys. **55**, 2014 (1971).
3. P. B. DAVIES, R. M. NEUMANN, S. C. WOFSY, and W. KLEMPERER. J. Chem. Phys. **55**, 3564 (1971).
4. J. B. ANDERSON, R. P. ANDRES, and J. B. FENN. Adv. Chem. Phys. **10**, 275 (1966); J. B. ANDERSON. *In* Molecular beams and low density gas dynamics. *Edited by* P. P. Wegener. Dekker, New York, NY. 1974.
5. S. G. KUKOLICH and A. C. NELSON. J. Chem. Phys. **56**, 4446 (1972).
6. J. M. H. REIJNDERS, A. W. ELLENBROEK, and A. DYMANUS. Chem. Phys. Lett. **17**, 351 (1972); **26**, 470 (1974).
7. A. W. ELLENBROEK. Ph.D. Thesis. Katholieke Universiteit, Nijmegen, The Netherlands. 1977; A. W. ELLENBROEK and A. DYMANUS. Chem. Phys. **35**, 227 (1978).
8. U. BORKENHAGEN, H. MALTHAN, and J. P. TOENNIES. J. Chem. Phys. **63**, 3173 (1975).
9. W. L. MEERTS, G. TER HORST, J. M. L. J. REINARTZ, and A. DYMANUS. Chem. Phys. **35**, 253 (1978).
10. T. L. FOLLETT. Ph.D. Thesis. Harvard University, Cambridge, MA. 1970.
11. C. DEVERELL. Mol. Phys. **18**, 319 (1970).
12. I. OZIER and W. L. MEERTS. Phys. Rev. Lett. **40**, 226 (1978).
13. J. G. SMITH. Mol. Phys. **32**, 621 (1976).

14. R. H. KAGANN, I. OZIER, and M. C. L. GERRY. J. Mol. Spectrosc. **71**, 281 (1978).
15. T. AMANO and R. H. SCHWENDEMAN. J. Chem. Phys. **68**, 530 (1978).
16. F. H. DE LEEUW and A. DYMANUS. J. Mol. Spectrosc. **48**, 427 (1973).
17. N. F. RAMSEY. Molecular beams. Oxford University Press, London, England. 1956.
18. L. H. SCHARPEN, J. S. MUENTER, and V. W. LAURIE. J. Chem. Phys. **46**, 2431 (1967).
19. I. OZIER, L. M. CRAPO, and S. S. LEE. Phys. Rev. **172**, 63 (1968).
20. W. H. FLYGARE. J. Chem. Phys. **41**, 793 (1964).
21. H. L. TIGELAAR and W. H. FLYGARE. Chem. Phys. Lett. **7**, 254 (1970).
22. I. OZIER, L. M. CRAPO, J. W. CEDERBERG, and N. F. RAMSEY. Phys. Rev. Lett. **13**, 482 (1964).
23. D. ANDRYCHUK. Can. J. Phys. **29**, 151 (1951).
24. J. W. EMSLEY, J. FEENEY, and L. H. SUTCLIFFE. High resolution N.M.R. spectroscopy. Pergamon Press, Oxford, England. 1966.
25. D. A. HELMS and W. GORDY. J. Mol. Spectrosc. **66**, 206 (1977).
26. M. M. CRUTCHFIELD, C. H. DUNGAN, J. H. LETCHER, V. MARK, and J. R. VAN WAZER. $P^{31}$ nuclear magnetic resonance. Interscience, New York, NY. 1967.
27. P. K. BHATTACHARYYA and B. P. DAILEY. Mol. Phys. **28**, 209 (1974).
28. W. GORDY and R. L. COOK. Microwave molecular spectra. Interscience, New York, NY. 1970.
29. J. M. L. J. REINARTZ and A. DYMANUS. Chem. Phys. Lett. **24**, 346 (1974).
30. E. R. COHEN and B. N. TAYLOR. J. Phys. Chem. Ref. Data, **2**, 663 (1973).
31. S. M. FREUND, G. DUXBURY, M. RÖMHELD, J. T. TIEDJE, and T. OKA. J. Mol. Spectrosc. **52**, 38 (1974).
32. W. H. FLYGARE and R. C. BENSON. Mol. Phys. **20**, 225 (1971).
33. W. PANOFSKI and M. PHILIPS. Classical electricity and magnetism. Addison-Wesley Publishing Company, Inc. London, England. 1955. p. 330.
34. A. W. ELLENBROEK and A. DYMANUS. Chem. Phys. Lett. **42**, 303 (1976).
35. R. G. STONE, J. M. POCHAN, and W. H. FLYGARE. Inorg. Chem. **8**, 2647 (1969).
36. E. HIROTA. J. Mol. Spectrosc. **37**, 20 (1971).
37. Y. KAWASHIMA and A. P. COX. J. Mol. Spectrosc. **61**, 435 (1976).
38. M. L. GRENIER-BESSON. J. Phys. Radium, **21**, 555 (1960).
39. J. M. L. J. REINARTZ, W. L. MEERTS, and A. DYMANUS. Chem. Phys. Lett. **16**, 576 (1972).

## Appendix A: Stark Effect in a Symmetric Top Molecule

[A1] $$E_{ST} = E_{ST}^{(1)} + E_{ST}^{(2)} + E_{ST}^{(3)} + \ldots$$

[A2] $$E_{ST}^{(1)} = -\mu\varepsilon m_J K/J(J+1)$$

[A3] $$E_{ST}^{(2)} = \frac{\mu^2\varepsilon^2}{2hB_0}\left\{\frac{(J^2-K^2)(J^2-m_J^2)}{J^3(2J-1)(2J+1)} - \frac{[(J+1)^2-K^2][(J+1)^2-m_J^2]}{(J+1)^3(2J+1)(2J+3)}\right\} - 1/3(\alpha_{\parallel}-\alpha_{\perp})\varepsilon^2\frac{[3K^2-J(J+1)][3m_J^2-J(J+1)]}{J(J+1)(2J-1)(2J+3)}$$

[A4] $$E_{ST}^{(3)} = -\frac{m_J K\mu^3\varepsilon^3}{2(hB_0)^2}\left\{\frac{(J^2-K^2)(J^2-m_J^2)}{(J-1)J^5(J+1)(2J-1)(2J+1)} - \frac{[(J+1)^2-K^2][(J+1)^2-m_J^2]}{J(J+1)^5(J+2)(2J+1)(2J+3)}\right\}$$

In $E_{ST}^{(3)}$ the cross term $\mu(\alpha_{\parallel}-\alpha_{\perp})\varepsilon^3/hB_0$ has been omitted because its contribution is far below the present experimental accuracy.